CBN-05-13

CORNELL

LABORATORY OF ELEMENTARY PARTICLE PHYSICS

July 21, 2005

HIGH SPECTRAL BRIGHTNESS UPGRADE FOR CHESS, BASED ON THE ERL-INTENDED GUN AND CRYOMODULE

Richard Talman

ABSTRACT. A (relatively) inexpensive CHESS upgrade, to be referred to as as RCESR or RC (for rapid cycling) is proposed. The energy recovery principle is not employed, but the design is critically dependent on the electron gun under development for the ERL. (Essentially) no conventional construction is required, as the new synchrotron (S') and the new storage ring (CESR') take the places currently occupied by the originals.

Starting from a gun and injector cryomodule like that for the Cornell-ERL, after the beam is injected into a linac much like that under development for the ILC, it is accelerated to an energy of about 200 MeV and then single turn injection into S' at an energy high enough to give good injection efficiency (reliant on excellent gun emittance). From a time shortly after this, because of adiabatic damping, the aperture of S' is comfortably large and there is no further beam loss. After acceleration to nominal energy of 5 GeV, there is single turn beam transfer to CESR'. After circulating for several seconds the beam is dumped and the cycle repeated.

Both S' and CESR' have minimum emittance designs. For improved injection into S' its focusing will be only about half as strong as for CESR' but, otherwise, their magnets and arc optics will be similar. Other differences may result from eddy current and wall impedance considerations as well as insertion straight section requirements. The aperture of CESR' could be smaller than at present, but for impedance reasons, and to preserve the capability of going to higher energy, probably will not be.

By reducing the storage time to several seconds, the Touschek limit on charge density is greatly reduced, consistent with a large reduction in the beam emittance. Because of the strong focusing required for such emittance, the ramp time in the synchrotron needs to be long, matched to the Touschek lifetime at the design beam current and emittance.

With little conventional construction envisaged, the CESR' lattice can support at most two ultralong undulators. But the spectral brightness from an ordinary, few meter long, undulator will be some two orders of magnitude greater than that from the same undulator in the currently-specified Cornell-ERL. For this comparison identical charge per bunch and bunch spacing during beam burst from the electron gun are assumed. The proposed scheme allows significantly inferior beam emittance for the injected beam without substantial degradation in the achieved spectral brightness. Furthermore the gun duty factor is reduced by several orders of magnitude.

Operation with electron energy well above 5 GeV, for example up to 8 GeV, may be practical. This would allow high spectral brightness operation on the $n = 1$ undulator resonance for the most commonly required x-ray energies. But slower ramping or weaker focusing in the synchrotron may be required, as the quadrupoles in the synchrotron may already be near limits at 5 GeV.

Pulse-to-pulse injection jitter—a potential weakness of ERL operation—will be cancelled within a few turns by feedback, as in existing storage rings.

Quite apart from its eventual use as a high brightness x-ray source, because of its strong focusing and ultrasmall emittance, the configuration can serve as R&D for a two-stage positron beam cooler for the ILC.

Ultrashort-bunch operation in the multi-femtosecond range, an intriguing potential ERL capability, is probably not feasible in the scheme being described here.

Contents

1. Production of High Quality X-Ray Beams 4
1.1. A Formula for Spectral Brightness $\mathcal{B}$ 4
1.2. A Strategy to Maximize $\mathcal{B}$ 5
2. Proposed Acceleration Scenario 6
3. Power Considerations For X-Ray Source Operation 6
3.1. Average Power 6
3.2. Instantaneous Power 7
4. Critical Components and Parameter Dependencies 8
5. Low Emittance Lattice Design 10
6. Design Formulas For Trbojevic-Courant Lattice 12
6.1. Thin Quadrupole Formulation 12
6.2. Thick Lens Treatment and Nonlinear Optics 15
6.3. Zero Dispersion Straight Sections 17
7. Numerical Values of Lattice Parameters 19
8. Emittance Evolution During Acceleration 21
9. Touschek Lifetime Estimate 21
10. Performance as X-Ray Source 22
10.1. Spectral Brightness From Short Undulator 22
10.2. Refinement of Spectral Brightness Calculation 24

Bibliography 27

1. Production of High Quality X-Ray Beams

1.1. A Formula for Spectral Brightness $\mathcal{B}$. The "spectral brightness" $\mathcal{B}$ of an x-ray source measures a (relativistically invariant) density of photons in six-dimensional phase space. As such $\mathcal{B}$ is the number of photons inside a six dimensional volume $\mathcal{V}_3\mathcal{P}_3$ (sufficiently small that all photon distribution functions are more or less constant throughout) divided by $\mathcal{V}_3\mathcal{P}_3$. For x-rays produced in a storage ring, $\mathcal{B}$ is made large at least partly by permitting $\mathcal{V}_3\mathcal{P}_3$ to be chosen very small. Another figure of merit, the "flux" $\mathcal{F}$ is, crudely speaking, given by the product $\mathcal{F} \sim \mathcal{V}_3\mathcal{P}_3\mathcal{B}$.

When x-rays are used in a scientific experiment the volume of the sample being radiated can be compared to $\mathcal{V}_3\mathcal{P}_3$. A storage ring is not well matched, for example, to making dental x-rays because the sample size is very large and the large value of brightness over a small volume is inappropriate. In this case the flux $\mathcal{F}$ is a better measure than $\mathcal{B}$ of the usefulness of the source.

The real value of storage ring x-ray sources is in the opposite extreme, where the sample size is comparable to, or smaller than $\mathcal{V}_3\mathcal{P}_3$. At the risk of annoying some fraction of the x-ray community, in this report I will refer to this as the "physically important" regime of storage ring x-ray operation. Whether or not this opinion is valid, everything said in this report applies only to this case. (In truth, important x-ray experiments span such a broad range that it is not really valid to say that $\mathcal{B}$ is always more important than $\mathcal{F}$. The extreme position taken here is mainly to avoid the constant repetition of qualifying statements in the what follows.) As a result $\mathcal{B}$ will be taken as the figure of merit to be maximized and $\mathcal{F}$ will not be mentioned again.

Using updated terminology[1], a maxim heard in the x-ray field, "never trade flux for spectral brightness", may seem to contradict the previous paragraph. But it *does not*. When discussing an experiment in which x-rays are scattered from a small sample, the maxim could be re-expressed more carefully as "never trade more detected photons for fewer detected photons", which no one should disagree with. For experiments falling into this category the rate of detected photons is governed by $\mathcal{B}$ rather than by $\mathcal{F}$. In this sense the use of the word "flux" in "never trade flux etc. etc. " is simply misleading.

The master formula governing the spectral brightness of the x-ray beam produced by electron beam current I from the fundamental $n = 1$ undulator resonance, in an undulator having N_w periods, with undulator parameter K (assumed less than 1), possibly due to Krinsky[**1**], is[2]

$$\mathcal{B}_1 = \frac{2\times 10^{18}\, I(\mathrm{A})}{\epsilon_x(\mathrm{nm})\epsilon_y(\mathrm{nm})}\,\frac{N_w\,K^2}{1+K^2/2}\,\frac{\mathrm{photons}}{\mathrm{s\ mm^2\ mr^2\ 0.1\%BW}}. \tag{1}$$

Here ϵ_x and ϵ_y are un-normalized emittances. This formula describes the $n = 1$, monochromatic x-ray beam whose wavelength depends, among other things, on the undulator period λ_w.[3]

[1]Until recently, at least in Ithaca, the quantity $\mathcal{B}$ was referred to as "brilliance". But we are told that the now universally adopted convention is to refer to this quantity as "spectral brightness".

[2]The functional dependences in Eq. (1) are not controversial, but the multiplying factor may vary by a factor of two or so, depending on assumptions.

[3]Qualification: Eq. (1), especially its only-linear dependence on N_w, depends on relations between the angular spreads of the electron beam and the produced photon cone angle. These

In practice, especially for high energy x-rays, production from higher undulator resonances, $n = 3$, $n = 5$, or even higher, produces greater spectral brightness than does $n = 1$. To mask this dependence, from here on, the spectral brightness will be indicated by $\mathcal{B}$ rather than by $\mathcal{B}_1$. Achievable values of $\mathcal{B}_n$ are given later.

1.2. A Strategy to Maximize $\mathcal{B}$. With B declared to be of pre-eminent importance, it is clear from Eq. (1) that I should be maximized consistent with ϵ_x and ϵ_y being minimized. The spectral brightness is also influenced by *undulator* design and optimization, but those dependencies are neglected in this paper.

The theory of electron storage ring equilibration (due mainly to Sands) is well established, including formulas for ϵ_x and ϵ_y, along with lattice designs that minimize the emittances. One such design is spelled out in detail in a later section. Before going into analytic detail, only the following two effects are here promoted to *fundamental limitation* status:

- The basic approach to reducing ϵ_x and ϵ_y is to focus the beam more strongly. This stronger focusing inevitably leads to reduced dynamic acceptance. With care, the equilibrium beam size decreases more or less proportional to the dynamic aperture, which seems to augur success in reducing emittances. Unfortunately the need to inject beam into the storage ring limits this approach. Either the beam is too large initially, or the betatron oscillations imparted by multiturn injection set a limit on maximum focusing strength.
- Another limit, almost as important, is set by the so-called Touschek effect, an intrabeam scattering process in which individual particles are scattered and lost. This limits the degree to which the emittances, especially ϵ_y, can be reduced.

With these two effects taken to be the only *fundamental* limitations, the approach taken in this paper is to eliminate them both by taking the following steps:

- Start with small emittance beams. This is achieved by using the gun plus injector intended for ERL operation.[**2**][**3**]
- Avoid multiturn injection. By injecting directly onto the equilibrium orbit, injection-induced betatron oscillations are avoided.
- Defeat the Touschek effect by storing individual electrons for times measured only in tens of seconds, far shorter than current Touschek lifetimes. In this regime ϵ_x and ϵ_y can be reduced by big factors before the Touschek effect again becomes important.
- However, choose a storage time long enough to take advantage of the damping of ϵ_y to a small value characteristic of conventional light sources. The electron bunch equilibration time (measured in numbers of turns) is about $E_e/\Delta E_e \approx 5000/1.3 \approx 4000$ turns, where the energy loss per turn at $E_e = 5\,\mathrm{GeV}$ in the proposed lattice is $\Delta E_e \approx 1.3\,\mathrm{MeV}$. This "long storage time" condition is therefore satisfied by storing for times long compared to 10 ms.

---

relations are likely to be different for horizontal and vertical emittances in the ranges of interest for this report.

2. Proposed Acceleration Scenario

Schematically, the proposed acceleration sequence is essentially the same as the existing gun/linac/synchrotron/storage-ring facility at Wilson Lab. This is shown in FIG 1. However the timing sequence (shown in FIG 2) is very different. In particular, any single electron circulates in the storage ring (CESR') for several seconds, instead of for an hour.

Once every several seconds (in the range from 2 to 20) the gun produces a $2\,\mu$s-long batch of electron bunches with interbunch spacing corresponding to 1.3 GHz. These electrons are accelerated to, say, 200 MeV, in the injector linac, with average current during each batch being 0.1 A. This linac is quite similar in design to the TESLA/ILC linac currently under development. However, cycling at $0.05 - 0.5\,$Hz, its duty factor is far less than in the TESLA design 5 Hz rate. Also, with total length not being a significant consideration, energy gain per meter in the injector can be less by a substantial factor than in a linear collider. The cost of this injector will be high, especially if the injection energy is chosen well above 200 MeV, but part of the development cost could perhaps be justified as R&D for the International Linear Collider.

After injection into synchrotron S', the electrons are accelerated up to a maximum energy taken nominally to be 5 GeV. This acceleration is performed in the element labeled S'-RF in the figure. This superconducting linac resembles the ERL injector linac. It has to be capable of accelerating an 0.1 A beam on a nearly-CW basis. Compared to ERL operation, though the duty factor reduction is modest—by a factor of only about two depending on the magnetic field cycle of S'—there are more important relaxations. The required longitudinal gradient is small and there is no minimum gradient imposed by space charge considerations. Compared to the ERL injector linac, the gradient of S'-RF can therefore be much less, perhaps by a factor of ten. Reducing the gradient incurs only the construction costs of more cryomodules and of taking up more space in the synchrotron.

At full energy the $2\,\mu$s batch of electrons is extracted from S' and single-turn injected into CESR', which should perhaps be referred to now as CHESS'. The same pulsed inflector into CHESS' that injects the present batch also ejects the previous batch, which is conveyed to the beam dump. During smooth operation this beam transfer should be invisible to x-ray users of CHESS'. There will, of course, need to be a gap of, say, 200 ns, to allow for turn on and turn off of the inflector/ejector. Injection jitter into CESR' can be eliminated immediately by single turn feedback.

There are no challenging acceleration components needed for CHESS'. Theoretical questions concerning emittance preservation, halo formation, insertion sections and so on are discussed in other sections of this report.

3. Power Considerations For X-Ray Source Operation

3.1. Average Power. In this section the rationale for the proposed design is discussed using "ballpark" parameter values. They are not supposed to be optimal but are adopted to simplify discussion.

The original rationale for building an ERL at Cornell (or elsewhere) went as follows. One wants to have a relatively high electron current such as $I \overset{e.g.}{=} 0.1\,$A at an electron energy $E_e \overset{e.g.}{=} 5\,$GeV. This corresponds to a supplied power of 500 MW, which is impractically large by a factor of at least one hundred. For purposes of

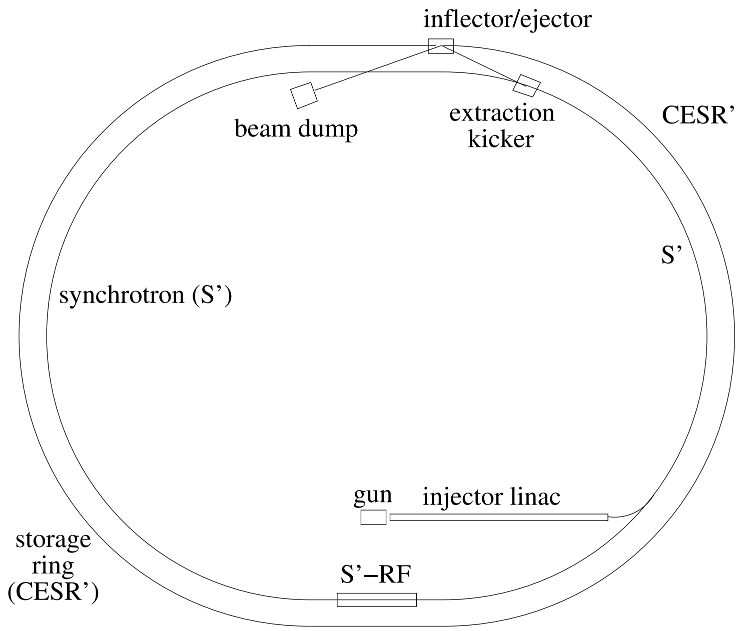

FIGURE 1. Schematic layout of the full acceleration system.

this paper let us strive for reduction of this power by a factor of at least one thousand. (Since the power radiated in undulators is expected to approach a megawatt, there is little justification for striving for a power reduction factor greater than one thousand.) In the ERL design a power reduction factor in the range from one hundred to one thousand is obtained by decelerating the electrons to recover most of their energy. In the scheme described here the reduction factor is achieved by reducing the *number* of electrons accelerated per second by a factor greater than one thousand—more than a million in fact.

In round numbers the revolution period of electrons in the Wilson tunnel is $T_{\rm rev.} \approx 2\,\mu$s, which gives 500,000 turns per second. In the proposed "rapid cycling" approach the electrons are dumped from CESR' every $T_{\rm cycle} \approx 2-20\,$s, after having completed $N_{\rm cycle} = 10^6 - 10^7$ turns. This will have abundantly achieved the factor of at least one thousand power reduction called for above.

Since the electron gun and injector are required only every several seconds, their duty factors, and hence their power consumption, will have been reduced by a big factor compared to the ERL. (As a further aside, this should give a major improvement in gun cathode life.)

Completing the argument of the first paragraph of this section, the nominal average power delivered to the beam and dumped at full energy will be $50-500\,$W.

3.2. Instantaneous Power. Continuing with the parameters assigned tentatively in the previous section, for ease of comparison with the existing ERL design, let us copy parameters from that source: the same beam current $I = 0.1\,$A; the same bunch bunch repetition rate $f_{\rm bunch} = 1.3\,$GHz; and the same charge per bunch $Q_1 = 77\,$pC.

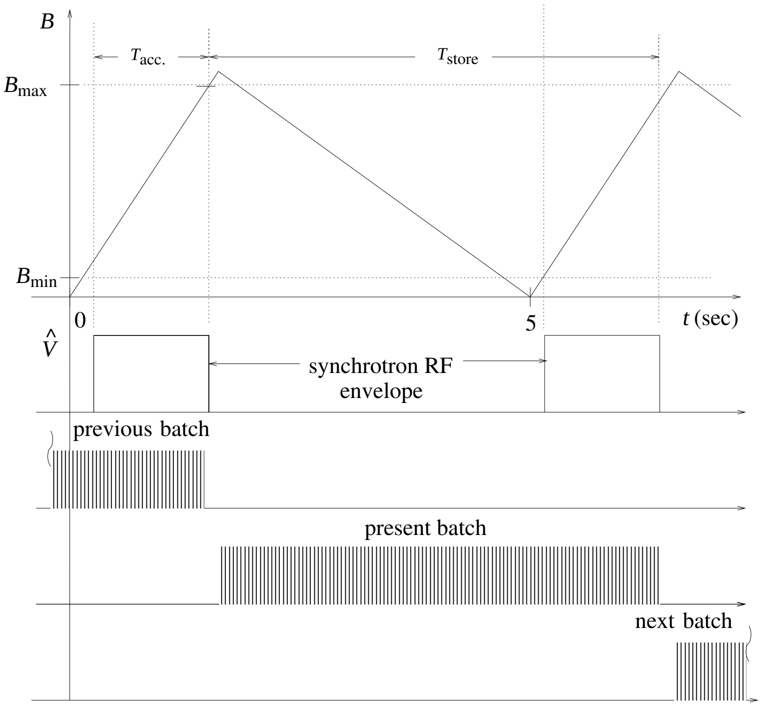

FIGURE 2. Acceleration cycle showing the synchrotron (S') magnetic field, the S'-RF modulation $\hat{V}$, and the bunch pattern in CESR'/CHESS'. The cycle time T_C, labelled 5 s in the figure, is expected to be in the range from 2 to 20 seconds.

The acceleration cycle shown in FIG 2 has been chosen so slow that energy gain per turn requirements in S' are modest, both for acceleration and to replace synchrotron radiation power loss—comfortably less than what is provided by one ERL injection cryomodule, some parameters of which are: five 1300 MHz 2-cell cavities, each producing 1 MeV of acceleration, for a power transfer to the beam of 100 kW at 0.1 A; length approximately 1 m. The RF acceleration in the synchrotron can therefore be provided by a one (or, for above-5 GeV operation, a small number) of such modules, perhaps located at the same positions as in the present synchrotron.

4. Critical Components and Parameter Dependencies

Some elements of the proposed scheme are "conservative" only in the sense of trusting that the specifications for the Cornell ERL are conservative. Some of the critical components and theoretical issues are listed here:

- As with the ERL, excellent gun performance is the *sine qua non* for operation at the design spectral brightness. In detail the dependence on gun specifications is different for the two schemes.
- The effect of reducing the gun current is quite different in the ERL and the present proposal. One expects that reduced gun current will be accompanied by reduced emittance. The ERL can take advantages of reduced ϵ_x

to recover the design brightness. The proposed scheme cannot do this; its achieved brightness simply tracks the gun current.

- In the ERL the ultimate brightness tracks the (inverse-squared) emittance faithfully. In contrast, the proposed design could compensate for excess emittance by increasing the synchrotron aperture or injection energy. At the design injection current this could recover the design brightness. Compared to the gun specifications assumed here, electron sources with similar bunching, charge per bunch and/or average current roughly ten times greater, and emittances roughly ten times worse, are described, for example, by M. Borland et al.[**4**] and by R. Sheffield et al.[**5**]. Simulations by Bazarov and Sinclair[**2**] predict emittances more or less proportional to charge per bunch, which is consistent with results in the papers of Borland and of Sheffield.
- The injector linac will be expensive, depending particularly on its energy, which is assumed to be at least 200 MeV. The critical front end will however be available upon ERL-Phase I(a) completion. The extra cost will come from acceleration from 10 MeV to 200 MeV which will, however, be at very low duty factor. Because of the high pulsed current requirement, a linac frequency much lower than the present Wilson Lab copper linac seems to be called for, but it need not be superconducting.
- As explained previously, an S'-RF unit resembles the ERL injector cryomodule quite closely as it has to operate almost CW at high beam current.
- To obtain the small value of ϵ_x in the present design requires an extremely high horizontal tune Q_x (as Table 1 shows.) According to the tracking simulation the resulting aperture is adequate, but further confirmation of this result is clearly required.
- Because of their ultrashort focal lengths, the synchrotron quadrupoles are challenging. Their high inductances will limit the ramp rate. This is why the total cycle time may have to be as long as $T_{\rm cycle} = 20\,$s. A further increase of $T_{\rm cycle}$ is likely to bring the Touschek effect back into play. Certainly a shorter value, such as $T_{\rm cycle} \approx 2\,$s would be preferable for the overall performance of the scheme.
- Multibunch instability in the synchrotron will have the same effect as reduced gun current. If the synchroton current is limited to a value less than the 100 mA assumed here, the spectral brightness will be reduced proportionally.
- To achieve small emittances in CESR' its focusing needs to be even stronger than in S'. From Table 1 the strongest quadrupole has strength $q_2 = 1.25\,\mathrm{m}^{-1}$, and length 0.33 m. This requires a pole tip field $B_{\rm pole}[\mathrm{Tesla}] = 0.63\,R_Q[\mathrm{cm}]$ where R_Q is the pole radius. How big R_Q must be depends on beam impedance considerations. If the quadrupoles in the favored $L_C = 6\,$m lattice are too strong, L_C could, for example, be doubled. This would reduce the quadrupole gradients by a (welcome) factor of four. But the weakened focusing would give a factor of eight increase in ϵ_x and a factor of 64 reduction in spectral brightness.
- As already stated, because of the ramping requirement, the focusing in S' will be made weaker than in CESR'. This causes no degradation of

overall performance. In fact it improves injection into S'. The effect of increased cell length is to increase the transverse beam size by a factor of roughly three during beam transfer from S' to CESR'. From Table 2 it can be seen that this increase can easily be tolerated without affecting the transfer efficiency. Increased aperture also improves injection into S' and may permit the injection energy to be reduced. This is investigated in Table 3.

5. Low Emittance Lattice Design

D. Trbocevic and E. Courant[**6**] describe a lattice design which minimizes the emittance (under their assumed hypotheses.) Their cell configuration is shown in FIG 3. There is a single dipole magnet in each cell, but it is convenient to regard the cell ends as occurring at the dipole center, as shown in the lower part of the figure.

The main results of the T-C paper can be distilled into the following few formulas. The horizontal emittance is given by

$$\epsilon_x = \frac{C_q \gamma^2}{J_x \rho} \mathcal{H}, \tag{2}$$

where $C_q = 3.84\ 10^{-13}\,\mathrm{m}$, $\gamma = E_0/(mc^2) = 0.978 \times 10^4$ for $E_0 = 5\,\mathrm{Gev}$, J_x, the partition number, can, for present purposes, be taken to be 1, and ρ is the bend radius in bending magnets. The factor $\mathcal{H}$, known as Sands's "curly H", is given in terms of Twiss functions and dispersion function η by

$$\mathcal{H} = \gamma_x \eta^2 + 2\alpha_x \eta\eta' + \beta_x {\eta'}^2. \tag{3}$$

Starting from their assumed values β_0 and η_0 at the origin, the s-dependences of β and η within the dipole are

$$\beta = \beta_0 + \frac{s^2}{\beta_0}, \quad \alpha \equiv -\frac{\beta'}{2} = -\frac{s}{\beta_0}, \quad \eta = \eta_0 + \frac{s^2}{2\rho}, \tag{4}$$

and the mean value of curly-H is given by

$$\begin{aligned} <\mathcal{H}> &= \frac{1}{L}\int_{-L/2}^{L/2} \frac{\eta^2 + (\eta\alpha + \eta'\beta)^2}{\beta}\, ds \\ &= \frac{\eta_0^2 - \theta\eta_0 L/12 + \theta^2 L^2/320}{\beta_0} + \frac{\theta_0^2 \beta_0}{12}, \end{aligned} \tag{5}$$

where L is the length of the bending magnet and $\theta = L/\rho$ is the the total bend angle in the magnet. The T-C mimimization procedure is to select values of β_0 and η_0 that minimize $<\mathcal{H}>$ with L and θ fixed. The result is

$$\beta_0 = \frac{L}{2\sqrt{15}}, \quad \eta_0 = \frac{\theta L}{24}, \quad <\mathcal{H}> = \frac{\sqrt{15}}{180} L\theta^2 = \frac{\sqrt{15}}{180} \rho\theta^3 \ . \tag{6}$$

All that remains is to adjust lattice parameters to match these values of β_0 and η_0. These conditions fix the lattice design, modulo a certain amount of freedom in choosing element lengths and locations. Without providing details, Trbojevic and Courant exhibit one cell design that meets the requirements. In the next section

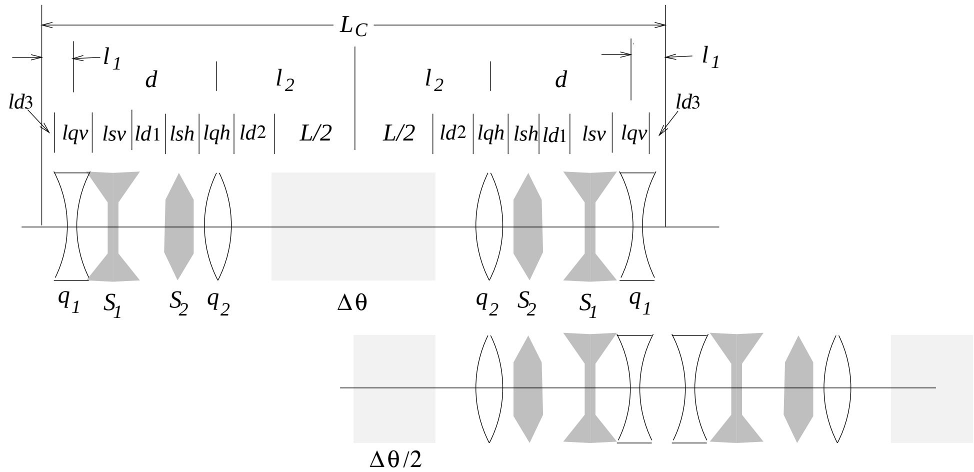

FIGURE 3. Thick and thin lens lengths and strengths for Trbojevic-Courant minimum emittance cell. The lower element ordering is convenient for relating design values of β_0 and η_0 to the Twiss functions of sectors consisting of repeated cells. The rectangular shaded region represents a bend magnet and the angular figures represent sextupoles. As the lenses are drawn, it is horizontal optics being illustrated. The parameter $ld3$, though tentatively set to zero, is available for flexibility.

I give a more detailed design prescription for design of individual cells and for the lattice as a whole.[4]

The parameter of greatest interest, the horizontal emittance ϵ_x, can be obtained using Eqs. (2) and (6);

$$\epsilon_x = \frac{C_q\gamma^2}{J_x}\frac{\sqrt{15}}{180}\left(\frac{2\pi}{N_C}\right)^3 \quad \left(\overset{e.g.}{=} 1.96\times 10^{-10}\left(\frac{100}{N_C}\right)^3 \text{m-rad}\right), \tag{7}$$

where N_C is the number of full cells in the lattice. The numerical estimate given here is based on parameter values given in Table 1. The length and strength parameters in this table are calculated in the next section.

The calculation described so far has concentrated on horizontal emittance ϵ_x, as is appropriate for the conventional hour-long type electron storage rings that have been constructed in the past. In such rings, over times large compared to 10 milliseconds, ϵ_x evolves toward the value given in Eq. (7). In multiturn injection this will normally constitute *shrinkage*, but in single turn injection from a low emittance source it is more likely to be *growth*. Meanwhile the vertical emittance ϵ_y damps down to a (typically) much smaller value, which depends on imperfections such as coupling and vertical dispersion.

[4]An earlier version of the discussion in this section was distributed in 2004 as lecture notes for Physics 689. The discussion here has profited from the work of Karl Smolenski, which he presented in the form of an oral and a written final assignment.

6. Design Formulas For Trbojevic-Courant Lattice

6.1. Thin Quadrupole Formulation. Though the T-C prescription certainly minimizes $< \mathcal{H} >$ under the assumed hypotheses, this is not quite equivalent to minimizing ϵ_x in a practical lattice intended to fit in an existing circular tunnel, having circumference $\mathcal{C}$, such as at the Wilson Lab. To avoid worrying about sections needed for RF accelerating structures, wigglers or undulators, instrumentation, etc., let us introduce an "arc circumference" $\mathcal{C}_a \overset{e.g.}{=} 660\,\mathrm{m}$, that leaves length $\mathcal{C} - \mathcal{C}_a \approx 100\,\mathrm{m}$ available for miscellaneous elements. By far the most important design choice is that of cell length L_C or, equivalently, the number of cells N_C. These are related by

$$\theta = \frac{2\pi}{N_C}, \quad \text{and} \quad L_C = \frac{\mathcal{C}_a}{N_C}. \tag{8}$$

From this and the last of Eqs. (6) the emittance apparently varies as N_C^{-3}, but considerations not included in the discussion so far will set a set a practical upper limit on N_C or, equivalently, a lower limit on L_C.

Another effect worth mentioning is that, because of the factor ρ in the denominator of Eq. (2), minimizing $\mathcal{H}$ is not equivalent to minimizing ϵ_x. In terms of quantities defined so far, ρ is given by[5]

$$\rho = \frac{\mathcal{C}_a}{2\pi}\frac{L}{L_C}, \tag{9}$$

To the extent that L fills most of the cell length L_C, minimizing $\mathcal{H}$ is equivalent to minimizing ϵ_x but, especially as L_C is reduced, an increasingly large fraction of the cell is required for the quadrupoles and sextupoles that are needed to achieve the optimal values of β_0 and η_0. This leads to difficult dependencies, even in designing the linear optics, and the ultimate limit is set by nonlinear effects that can only be studied by simulation using particle tracking. (This should not be surprising if the length required for sextupoles exceeds the quadrupole length allotment. A possibility worth considering is to have one of the sextupole types be built into the dipoles, by shaping their poles. This would bring in nonlinear complications even in the analysis of the effects of quantum fluctuations in the synchrotron radiation, but the formalism for treating such effects is well established.) Obviously a final design will have to be the result of iterating these steps. In this paper I make only a single, tentative, choice of element locations, and study the performance as a function of L_C. I do not attempt to iterate beyond this first cut design, and I ignore complications such as fringe fields or the circumference allotment required for magnet ends.

Especially for conventional (multi-hour) storage ring design, other, more important, phenomena limit the maximum practical value of N_C. With increasing N_C the dynamic aperture decreases. Though the equilibrium beam size decreases more or less proportionally, the effective beam size during multiturn injection is independent of N_C and injection efficiency decreases with increasing N_C. Yet another similar limitation results from the Touschek effect in which an individual electron occasionally receives a kick sending it into a halo where it may be lost. For the

[5]Following Sands originally, as do T-C, this paper assumes an "isomagnetic" lattice in which the magnetic field has the same value everywhere except where it vanishes.

scheme proposed here the occasional particle will be lost because of the Touschek effect, but this will have little effect on operations.

For linear lattice design, following Trbojevic and Courant, though the bend region is crucial to evolution of the dispersion function, its "optical" effect on $\beta_x(s)$ is ignored. Also the quadrupoles are initially treated as thin lenses—this assumption is retracted in a final design step using the TEAPOT program (and eventually, UAL) to study the dynamic acceptance of the lattice.

Trbojevic and Courant are correct in asserting that there are enough free parameters to allow the β_x and η_x-function values to be achieved. They do not, however, analyse the restriction that follows from the need for the vertical motion to be stable. In fact, the simplest solutions have both q_1 and q_2 horizontally focusing, which is obviously unsatisfactory. Hence, in seeking solutions, one should certainly impose the condition $q_1 q_2 < 0$. After a certain amount of trial and error, it appeared that the best place for the vertical focusing quad is as far from the dipole as possible. This suggested the virtue of pushing it to the very end of the cell, as shown in FIG 3 for $ld3 = 0$. This has the further virtue of reducing the number of vertical focusing quads by a factor of two, by permitting elements from adjacent cells to be combined. The T-C conditions can be met in this case, while retaining vertical stability. There are indications though, that the "stability window" is very small. For example, the lattice is stable for q_1 being a thick lens, but it becomes unstable in the limit that the q_1 lenses on the boundaries between cells are combined into a shared thin lens. It remains to be seen whether this "flaky behavior" makes the nonlinear optics and dynamic acceptance unsatisfactory. It may be that the T-C lattice is "unnecessarily good" and that accepting somewhat higher emittance would lead to more robust optics.

Transfer matrix analysis of the thin lens doublet configuration shown in the left half of the upper lattice cell shown in FIG 3 yields

$$\begin{pmatrix} X_x & X_{x'} \\ F_x & F_{x'} \end{pmatrix} = \begin{pmatrix} 1 & l_2 \\ 0 & 1 \end{pmatrix} \begin{pmatrix} 1 & 0 \\ -q_2 & 1 \end{pmatrix} \begin{pmatrix} 1 & d \\ 0 & 1 \end{pmatrix} \begin{pmatrix} 1 & 0 \\ -q_1 & 1 \end{pmatrix} \begin{pmatrix} 1 & l_1 \\ 0 & 1 \end{pmatrix}, \tag{10}$$
$$\begin{pmatrix} Y_y & Y_{y'} \\ G_y & G_{y'} \end{pmatrix} = \begin{pmatrix} 1 & l_2 \\ 0 & 1 \end{pmatrix} \begin{pmatrix} 1 & 0 \\ q_2 & 1 \end{pmatrix} \begin{pmatrix} 1 & d \\ 0 & 1 \end{pmatrix} \begin{pmatrix} 1 & 0 \\ q_1 & 1 \end{pmatrix} \begin{pmatrix} 1 & l_1 \\ 0 & 1 \end{pmatrix}.$$

Notice that *positive* q values correspond to *horizontal focusing*, so $q_1 < 0$ and $q_2 > 0$. Completing the multiplications yields, in the horizontal plane,

$$\begin{aligned} X_x &= 1 - (d + l_2)q_1 - l_2 q_2 + d l_2 q_1 q_2 \\ X_{x'} &= l_1 + d + l_2 - l_1(d + l_2)q_1 - (l_1 + d)l_2 q_2 + l_1 d l_2 q_1 q_2 \\ F_x &= -q_1 - q_2 + d q_1 q_2 \\ F_{x'} &= 1 - l_1 q_1 - (l_1 + d)q_2 + l_1 d q_1 q_2. \end{aligned} \tag{11}$$

In the vertical plane all negative signs are replaced by positive signs;

$$\begin{aligned} Y_y &= 1 + (d + l_2)q_1 + l_2 q_2 + d l_2 q_1 q_2 \\ Y_{y'} &= l_1 + d + l_2 + l_1(d + l_2)q_1 + (l_1 + d)l_2 q_2 + l_1 d l_2 q_1 q_2 \\ G_y &= q_1 + q_2 + d q_1 q_2 \\ G_{y'} &= 1 + l_1 q_1 + (l_1 + d)q_2 + l_1 d q_1 q_2. \end{aligned} \tag{12}$$

Letting $\mathbf{X}$ be the 4×4 transfer matrix of the left half cell in the upper part of FIG 3, the input and output coordinates of a general trajectory are related by the usual relations,

$$\mathbf{x}_{\text{out}} = \mathbf{X}\mathbf{x}_{\text{in}}, \text{ and } \mathbf{x}_{\text{in}} = \mathbf{X}^{-1}\mathbf{x}_{\text{out}}. \tag{13}$$

The second half of the cell consists of the same elements, but encountered in the opposite order. Let $\check{\mathbf{X}}$ stand for the transfer matrix of this sequence. Symmetry under this reflection is closely related to time reversal invariance that relates forward and backward evolving trajectories. To express this mathematically, introduce a matrix σ_3 that reverses the slopes,

$$\begin{pmatrix} x \\ -x' \\ y \\ -y' \end{pmatrix} = \begin{pmatrix} 1 & 0 & 0 & 0 \\ 0 & -1 & 0 & 0 \\ 0 & 0 & 1 & 0 \\ 0 & 0 & 0 & -1 \end{pmatrix} \begin{pmatrix} x \\ x' \\ y \\ y' \end{pmatrix} \equiv \sigma_3 \mathbf{x}, \tag{14}$$

From the vector $\mathbf{x}_{\text{out}}$ appearing in Eq. (13), form the vector $\sigma_3\mathbf{x}_{\text{out}}$ and take it as input to the reversed-order half-cell. By symmetry, after propagating through the half-cell, one should recover $\sigma_3\mathbf{x}_{\text{in}}$, where $\mathbf{x}_{\text{in}}$ appears in Eq. (13). That is

$$\sigma_3\mathbf{X}^{-1}\mathbf{x}_{\text{out}} = \sigma_3\mathbf{x}_{\text{in}} = \check{\mathbf{X}}\sigma_3\mathbf{x}_{\text{out}}, \tag{15}$$

and it follows from this that

$$\check{\mathbf{X}} = \sigma_3\mathbf{X}^{-1}\sigma_3. \tag{16}$$

Because the determinants are equal to 1, the inverse matrices are given by

$$\begin{pmatrix} X_x & X_{x'} \\ F_x & F_{x'} \end{pmatrix}^{-1} = \begin{pmatrix} F_{x'} & -X_{x'} \\ -F_x & X_x \end{pmatrix}, \quad \begin{pmatrix} Y_y & Y_{y'} \\ G_y & G_{y'} \end{pmatrix}^{-1} = \begin{pmatrix} G_{y'} & -Y_{y'} \\ -G_y & Y_y \end{pmatrix}. \tag{17}$$

As mentioned before, it is most convenient to select the center of the dipole magnet as origin. The transfer matrix $\mathbf{M}$, through the full cell from this point, is given by (18)

$$\mathbf{M} = \mathbf{X}\check{\mathbf{X}} = \begin{pmatrix} X_xF_{x'} + X_{x'}F_x & 2X_xX_{x'} & 0 & 0 \\ 2F_xF_{x'} & X_xF_{x'} + X_{x'}F_x & 0 & 0 \\ 0 & 0 & Y_yG_{y'} + Y_{y'}G_y & 2Y_yY_{y'} \\ 0 & 0 & 2G_yG_{y'} & Y_yG_{y'} + Y_{y'}G_y \end{pmatrix}.$$

If the cell is part of a periodic lattice, its transfer matrix can be written in the form

$$\mathbf{M} = \begin{pmatrix} \cos\mu_x & \beta_x \sin\mu_x & 0 & 0 \\ -\sin\mu_x/\beta_x & \cos\mu_x & 0 & 0 \\ 0 & 0 & \cos\mu_y & \beta_y\sin\mu_y \\ 0 & 0 & -\sin\mu_y/\beta_y & \cos\mu_y \end{pmatrix}. \tag{19}$$

Note that the vanishing of the α's is consistent with Eq. (18) because the 11,22 and 33,44 element are pairwise equal. The reason for this is that the full cell is invariant to element reversal, so Eq. (16) implies that $\mathbf{M} = \sigma_3\mathbf{M}^{-1}\sigma_3$. We have therefore obtained formulas for the Twiss parameters at the cell ends;

$$\cos\mu_x = X_xF_{x'} + X_{x'}F_x, \quad \sin^2\mu_x = -4X_xX_{x'}F_xF_{x'}, \beta_x^2 = -\frac{X_xX_{x'}}{F_xF_{x'}},$$

$$\cos\mu_y = Y_yG_{y'} + Y_{y'}G_y, \quad \sin^2\mu_y = -4Y_yY_{y'}G_yG_{y'}, \beta_y^2 = -\frac{Y_yY_{y'}}{G_yG_{y'}}. \tag{20}$$

Because of the multiple-valued nature of inverse trigonometric functions, a certain amount of care is required in extracting the Twiss parameters from these relation. For the numerical values given in Table 1:

$$Q_x = 1 - \frac{\cos^{-1}(X_x F_{x'} + X_{x'} F_x)}{2\pi} = 1 - \frac{\sin^{-1}(\sqrt{-4X_x X_{x'} F_x F_{x'}})}{2\pi},$$
$$Q_y = \frac{\cos^{-1}(Y_y G_{y'} + Y_{y'} G_y)}{2\pi} = 0.5 - \frac{\sin^{-1}(-\sqrt{-4Y_y Y_{y'} G_y G_{y'}})}{2\pi}. \tag{21}$$

The T-C requirement on β_0 can be expressed by combining this result with the first of Eqs. (6) to yield the significant design formula;

$$\sqrt{-\frac{X_x X_{x'}}{F_x F_{x'}}} = \frac{L}{2\sqrt{15}}. \tag{22}$$

If we regard all lengths as fixed, then this equation provides one of the two conditions needed to fix the adjustable parameters q_1 and q_2.

Except within the dipole region, the dispersion function has the same s-dependence as does a particle trajectory. At the dipole end, using Eq. (4), we have $\eta(L/2) = \eta_0 + L\theta/4$ and $\eta'(L/2) = \theta$. Since $\eta(s)$ must have even symmetry about the cell center, and $\eta'(s)$ is odd, we must have

$$\begin{pmatrix} \eta_0 + L\theta/8 \\ -\theta/2 \end{pmatrix} = \mathbf{M}_{l_2 \to l_2 - L/2} \begin{pmatrix} \eta_0 + L\theta/8 \\ \theta/2 \end{pmatrix}, \tag{23}$$

because the transfer matrix through the bend-less section differs from the full transfer matrix only by the reduced entrance and exit distances indicated by the subscript on $\mathbf{M}$. This equation, along with Eq. (22), fix both q_1 and q_2. (The redundancy resulting because Eq. (23) contains two equations provides a consistency check.)

6.2. Thick Lens Treatment and Nonlinear Optics. Thick lens optical functions are shown in FIG 4 and FIG 5 and also in the form of numbers at the bottom of Table 1. The η_0 thick lens values are quite close to the design values. The β_x values are less good, typically too large by 50%, so the emittances would be increased by about the same factor. The values of β_y are even worse, too great by roughly a factor of two.

The required sextupole strengths (needed to compensate chromaticity) increase rapidly with tune. Because sextupole strengths vary inversely with bore diameter squared, it may be sextupole strengths that limit the cell length.

A dimensionally consistent (over-)estimate of dynamic aperture is q/S which, for CESR (the present version) would yield about 0.5 m. To estimate the dynamic acceptance of the proposed ring, sextupoles S_1 and S_2 have been adjusted to set both chromaticities to zero. The resulting sextupole strengths are shown near the bottom of the Table 1.[6] Values of the ratio q/S are also listed. From these numbers we have to expect dynamic apertures smaller than a centimeter. (As mentioned before, superimposing sextupole on the dipole may give an improvement.) In any case, when measured in units of beam σ's, the dynamic acceptance can be quite satisfactory because of the exceedingly low value of ϵ_x, since the needed aperture has a factor scaling as $\sqrt{\epsilon_x}$.

[6] One must beware a conventional factor $n! = 2$ that may or may not enter the definition of sextupole strength.

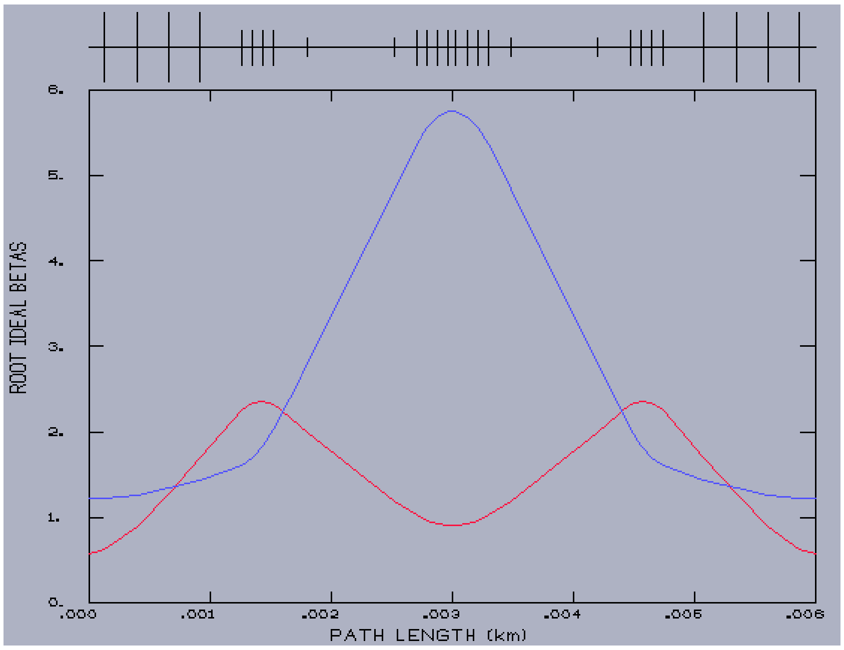

FIGURE 4. Functions $\sqrt{\beta_x(s)}$ and $\sqrt{\beta_y(s)}$ for the $L_C = 6\,\mathrm{m}$ case.

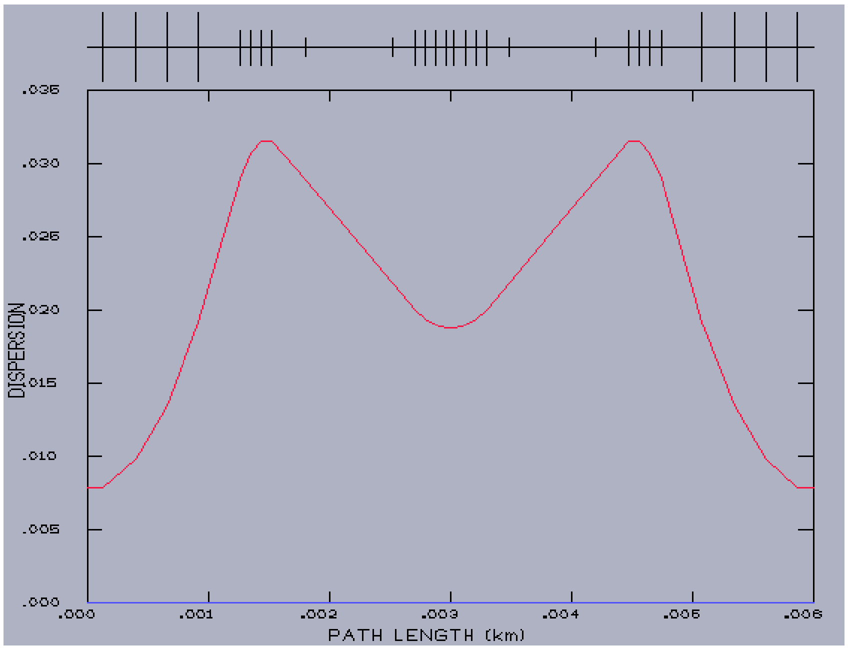

FIGURE 5. Dispersion function $\eta(s)$ for the $L_C = 6\,\mathrm{m}$ case.

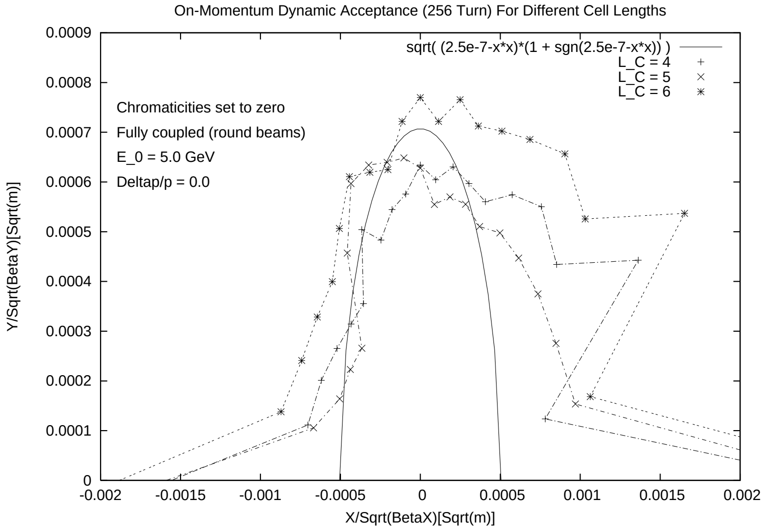

FIGURE 6. On-momentum transverse acceptance for $L_C = 4, 5$ and 6 m. Particles are launched from a dipole center with $x' = y' = 0$, with increasingly large amplitudes, for various rays emanating from the origin at various azimuthal angles. The maximum points for 256 turn stable motion are plotted at $x/\sqrt{\beta_x}, y/\sqrt{\beta_y}$. The smooth curve is an *ad hoc*, more or less maximal ellipse inscribed within the $L_C = 6$ m data.

The results of numerical tracking are shown in FIG 6 for on-momentum, and FIG 8 and FIG 7 for off-momentum. What is plotted are boundaries, in the x-y plane, inside which the motion is stable (for at least 256 turns) and outside which it is unstable. An example may be helpful in interpreting these graphs: consider the barely stable $\Delta p/p = 0$, $L_C = 6$ m point, with coordinates $x = 0$, $y/\sqrt{\beta_y} = 0.77 \times 10^{-3}\sqrt{\text{m}}$. From Table 1 one has $\beta_y = 4.1$ m, with the result that $y = 1.5$ mm. This point sets a vertical limit, at the dipole center, for a beam with large vertical motion (present, for example, because of coupling.) However, one is more concerned with the aperture at the vertical focusing quads where $\beta_y \approx 25$ m, and $y \approx 4$ mm.

6.3. Zero Dispersion Straight Sections. It is appropriate to install most insertion devices at positions of zero dispersion. In this section such a zero dispersion region is designed. A more practical design would include the vertical focusing due to the (presumed to be) undulator located in the straight section.

Within a pure dipole magnet the equation satisfied by the dispersion function is

$$\frac{d^2\eta}{ds^2} = \frac{1}{\rho} \quad \text{and hence} \quad \Delta\eta' = \frac{\Delta s}{\rho}\ . \tag{24}$$

In one T-C cell η' increases from $-\theta/2$ to $\theta/2$ in a magnet of length L. Correspondingly, η' would increase from 0 to $\theta/2$ in a magnet of length $L/2$. One therefore

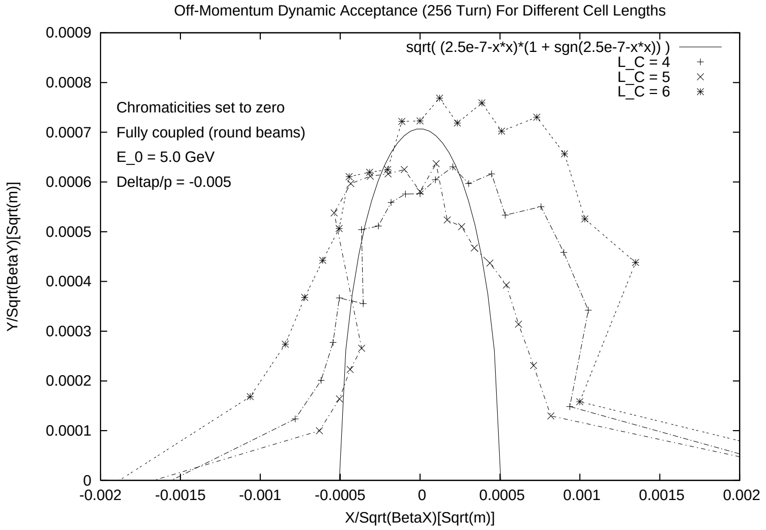

FIGURE 7. Off-momentum $\Delta p/p = -0.005$, transverse acceptance for $L_C = 4, 5$ and $6\,\mathrm{m}$.

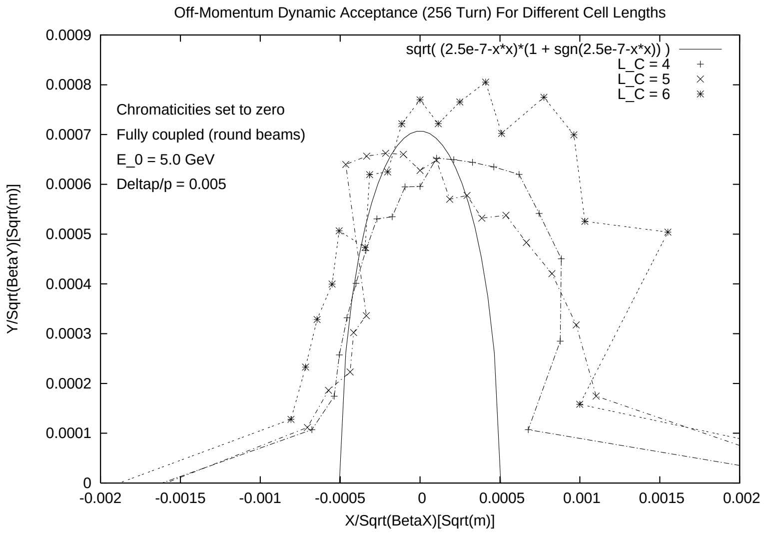

FIGURE 8. Off-momentum $\Delta p/p = 0.005$, transverse acceptance for $L_C = 4, 5$ and $6\,\mathrm{m}$.

envisages a dispersion matching cell that is identical to the T-C cell, with the exception that the magnet is only half-length, and is also appropriately located, with its entrance position at $s = \tilde{s}$ so that the dispersion function $\tilde{\eta}(L/2)$ (in the special cell) matches $\eta(L/2)$ (of the regular cell.) The condition for match is

$$\frac{(L/2)^2}{2\rho} + \frac{\theta}{2}\left(\frac{L}{2} - \tilde{s} - \frac{L}{2}\right) = \eta_0 + \frac{L\theta}{8}\ . \tag{25}$$

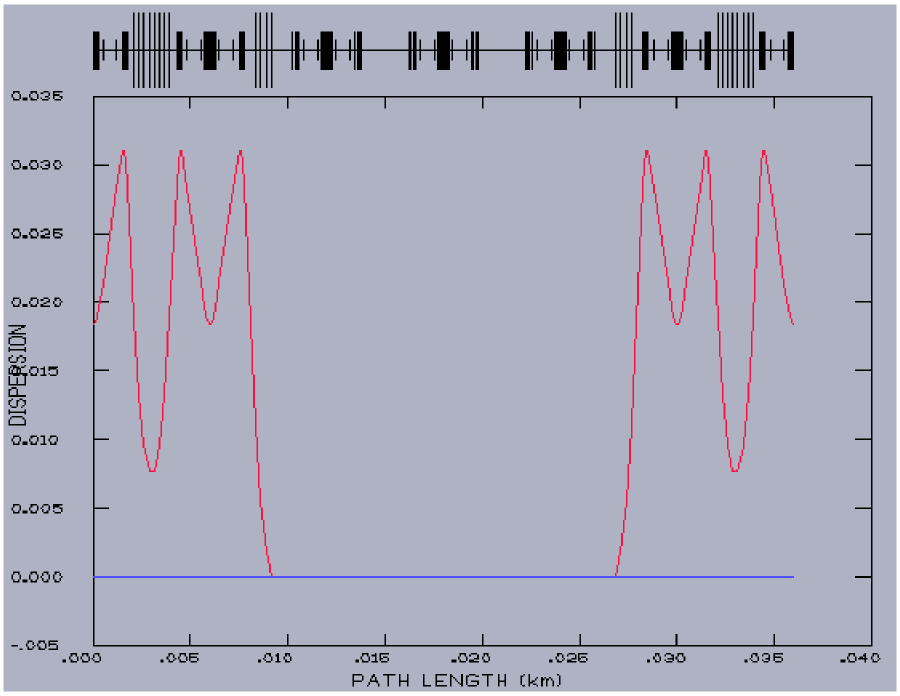

FIGURE 9. Six consecutive T-C cells, with the second and fifth cells modified to provide zero dispersion in the third and fourth cells.

In this equation one could substitute for η_0 using Eq. (6) but, since the thick lens and thin lens optics do not agree very well, we leave the condition as

$$\tilde{s} = -\frac{2\eta_0}{\theta}\ , \tag{26}$$

and anticipate fixing $\tilde{s}$ empirically, in the thick lens optics, to give perfect dispersion suppression. The optics for a sequence of six T-C cells, with dispersion suppressed in the central two, is shown in FIG 9.

7. Numerical Values of Lattice Parameters

The lattice plots exhibited so far have investigated cell length values $L_C = 4, 5, 6\,$m. The various performance requirements are satisfied by the $L_C = 6\,$m choice. Parameters for this case are shown in Table 1. After having fixed all length parameters, Eqs. (22) and (23), constrained by the requirement $q_1 q_2 > 0$, were solved using MAPLE. Because they are polynomial equations, MAPLE is able to solve the equations "exactly" without using numerical methods. This is not just apple-polishing since the desired solution can be picked automatically, circumventing the need to manually scrutinize all of the numerous solutions, some of which are complex, others unstable vertically.

TABLE 1. Numerical Values For the $L_C = 6\,\mathrm{m}$ Minimal Emittance Lattice.

parameter	unit	x-value	y-value
E_0	GeV	5.0	
$\mathcal{C}_a$		660.0	
ρ	m	36.765	
B	T	0.4536	
L_C	m	6.0	
N_C		110	
L	m	2.1	
θ	rad	.05712	
lqh	m	0.33	
lqv	m	0.33	
lsh	m	0.48	
lsv	m	0.30	
$ld1$	m	0.33	
$ld2$	m	0.18	
$ld3$	m	0.0	
l_1	m	0.165	
l_2	m	1.395	
d	m	1.44	
q_1,q_2	1/m	-0.5104	1.2511
β_x,β_y	m	0.2711	0.4097
η_0	m	.00500	
Q_x,Q_y	one cell	0.7902	0.4334
Q_x,Q_y	total	86.92	47.68
$< \mathcal{H} >$	$10^{-4}\,\mathrm{m}$	1.474	
ϵ_x	$10^{-10}\,\mathrm{m}$	1.474	
Thick Lens Analysis (param.'s as above)			
Q_x,Q_y	total	77.80	31.20
S_1,S_2	$1/m^2$	-27.15	35.02
η_0	m	0.00771	
β_x,β_y	m	0.3345	1.5348
q/S	mm	18.8	35.7

Assuming 5 GeV operation, since E, B and ρ values are the same for all cases, so are the following radiation quantities:

$$
\begin{aligned}
U_0 &= \text{energy radiated per turn} = 0.885 \times 10^{-4}\,\mathrm{m/GeV^3}\,\frac{5^4}{42} = 1.32\,\mathrm{MeV}\ , \\
u_c &= \text{critical energy} = 6.6\,\mathrm{keV}, \qquad (27)\\
\sigma_\delta &= \text{fractional energy spread} = 0.00066, \\
P_{\mathrm{tot}} &= \text{total radiated power} = 1.32\,(\mathrm{MW/A})\,I_{\mathrm{tot}}.
\end{aligned}
$$

8. Emittance Evolution During Acceleration

The so-called "normalized emittance" $\epsilon^{(n)}$, implicitly hides the beam size variation due to adiabatic damping. But there can also be shrinkage due to synchrotron radiation damping and growth due to quantum fluctuation. There will be transition from input-dominated emittance to radiation-dominated emittance during beam acceleration in S'. It will occur in the vicinity of the horizontal line shown in a table to be introduced shortly.

To determine whether the accelerator aperture is sufficiently large, after establishing the normalized emittance $\epsilon^{(n)}(\gamma)$, it is necessary to determine the "unnormalized emittance" $\epsilon(\gamma)$. These emittance are related by

$$\epsilon = \frac{\epsilon^{(n)}}{\gamma}. \tag{28}$$

FIG's 6, 7, and 8 are applicable to both S' and CHESS'. With $x/\sqrt{\beta_x}$ and $y/\sqrt{\beta_y}$ for axes, the same plots are applicable everywhere in both rings, for appropriate choice of beta functions. Treating these plots as "phase diagrams", contours separates stable phase (inside) from unstable phase (outside), for a particular choice of parameters.

These contours are roughly elliptical and, to simplify the discussion without making it less conservative for beams having height much less than width, the maximum amplitude contour can be replaced by an ellipse passing through the worst-case combination of x and y. Motion is stable through *all* the interior of this ellipse and unstable through *most* of its exterior. Such ellipses are shown in the figures. The way that this simplifies the discussion is that it relieves the need for discussing horizontal and vertical motion separately. The size of this ellipse is expressed by a value $\epsilon_{\mathrm{acc.}}$. This quantity has dimensions of length and is independent of the instantaneous beam energy of a beam being accelerated.

Of course, the physical dimensions of the beam vary as the beam accelerates. Detailed data describing the evolution of beam parameters throughout an acceleration cycle is given in Table 2, assuming $\epsilon_{\mathrm{acc.}} = (0.0005\sqrt{\mathrm{m}})^2 = 0.25\,\mu\mathrm{m}$. This value corresponds to the value used to calculate the smooth contours in FIG's 6, 7, and 8. For the numbers in Table 2 the injection energy would be chosen to be at least as high as 200 MeV, where the beam stay clear at injection into S' is 7σ, including momentum spread. More conservative injection would be at 300 MeV where the stay clear is 8.6σ. If neither of these is considered sufficiently conservative L_C would have to be increased from 6 m. The effects of such a change were discussed previously.

The data in Table 2 suggest that weaker focusing be used in the synchrotron than in CESR'. Table 3, with $L_C = 12\,\mathrm{m}$, is applicable to the synchrotron. For this table $\epsilon_{\mathrm{acc.}}$ was obtained by simple scaling rather than by tracking (which is what *should* be done.) According to the numbers in Table 3, for $L_C = 12\,\mathrm{m}$, transfer from S' to CESR' is satisfactory up to 8 GeV.

9. Touschek Lifetime Estimate

Results of some rudimentary Touschek effect calculations are shown in FIG 10. The formula labeled "Bruck"[**7**] comes from a chapter describing a theory due to Haissinski, in a book by Bruck. The formula labeled "LeDuff" comes from an article by C. Bocchetta[**8**]. These theories apparently differ primarily in their treatments

TABLE 2. Emittance evolution and aperture requirements during acceleration, assuming identical lattices for S' and CESR'. $\epsilon_{\rm in}^{(n)} = 2.0\,\mu$m, $\epsilon_{\rm acc.} = (0.0005\sqrt{\rm m})^2 = 0.25\,\mu$m. There is a transition somewhere near 1 GeV (roughly where the horizontal line is drawn part way down the table) where the equilibrium emittance first begins to dominate the injection emittance. Entries above this in the "equilibrium" columns are only academic, as are entries below this line in the "input" columns. ΔE_e is the energy loss per turn and τ is a characteristic damping time.

E_e GeV	ΔE_e MeV	τ s	$\epsilon_{\rm in}$ m	$\sqrt{\epsilon_{\rm acc.}/\epsilon_{\rm in}}$	$\epsilon_{\rm equi.}^{(n)}$ m	$\epsilon_{\rm equi.}$ m	$\sqrt{\epsilon_{\rm acc.}/\epsilon_{\rm equi.}}$
0.1	2.1E-7	1040	1.02E-8	4.95	1.15E-11	5.90E-14	2060
0.2	3.4E-6	130	5.11E-9	6.99	9.23E-11	2.36E-13	1030
0.3	1.7E-5	39	3.41E-9	8.57	3.12E-10	5.31E-13	686
0.4	5.4E-5	16	2.56E-9	9.89	7.38E-10	9.43E-13	512
0.5	1.3E-4	8.3	2.04E-9	11.1	1.44E-9	1.47E-12	412
0.7	5.1E-4	3.0	1.46E-9	13.1	3.96E-9	2.89E-12	294
1.0	2.1E-3	1.04	1.02E-9	15.6	1.15E-9	5.90E-12	206
1.5	1.1E-2	0.31	6.81E-10	19.2	3.89E-8	1.33E-11	137
2.0	3.4E-2	0.13	5.11E-10	22.1	9.23E-8	2.36E-11	103
3.0	0.171	0.039	3.41E-10	27.1	3.12E-7	5.31E-11	68
4.0	0.541	0.0163	2.56E-10	31.3	7.38E-7	9.43E-11	52
5.0	1.32	0.0083	2.04E-10	35	1.44E-6	1.47E-10	41.2
6.0	2.74	0.0048	1.70E-10	38	2.48E-6	2.12E-10	34.3
7.0	5.07	3.0E-3	1.46E-10	41	3.97E-6	2.89E-10	29.4
8.0	8.65	2.0E-3	1.28E-10	44	5.91E-6	3.77E-10	25.7

of dispersion. Since the LeDuff theory is more recent, it may be more reliable. The lifetime increases proportional to γ^4, or to an even higher power of γ, depending on assumptions concerning the beam σ's[**9**].

Experts in the field can undoubtedly produce far more reliable data than those in FIG 10. But, to support the present design, all that is needed is the observation that Touschek lifetimes for existing storage rings are measured in *hours*. The several *second* storage time in the present proposal assures the possibility of a huge reduction in beam emittances before the Touschek effect again limits operations. An uncertainty factor of two or more in the Touschek lifetime is somewhat irrelevant, since other factors are likely to set less optimistic lower limits on the emittances.

10. Performance as X-Ray Source

10.1. Spectral Brightness From Short Undulator. Using Eq. (1), a first, coarse, comparison between the spectral brilliance achievable from the x-ray source proposed here, and the proposed Cornell ERL source, can be made easily under the assumption of equal electron energy ($E_e = 5\,$GeV) and equal beam currents ($I = 0.1\,$A) in both cases. Using subscripts RC (for rapid cycling) and ERL,

$$\frac{\mathcal{B}_{\rm RC}}{\mathcal{B}_{\rm ERL}} = \frac{\epsilon_{x,{\rm ERL}}}{\epsilon_{x,{\rm RC}}}\frac{\epsilon_{y,{\rm ERL}}}{\epsilon_{y,{\rm RC}}} \approx \frac{2.0\,\mu{\rm m}}{1.44\,\mu{\rm m}}\,\frac{2.0\,\mu{\rm m}}{1.44\,\mu{\rm m}/100} \approx 190. \tag{29}$$

TABLE 3. Emittance evolution in synchrotron S', with its cell length taken to be $L_C = 12\,\mathrm{m}$, twice as great as in CESR'.

E_e GeV	ΔE_e MeV	τ s	ϵ_{in} m	$\sqrt{\epsilon_{\mathrm{acc.}}/\epsilon_{\mathrm{in}}}$	$\epsilon^{(n)}_{\mathrm{equi.}}$ m	$\epsilon_{\mathrm{equi.}}$ m	$\sqrt{\epsilon_{\mathrm{acc.}}/\epsilon_{\mathrm{equi.}}}$
0.1	2.1E-7	1040	1.02E-8	9.89	9.23E-11	4.72E-13	1460
0.2	3.4E-6	130	5.11E-9	14.0	7.38E-10	1.89E-12	728
0.3	1.7E-5	39	3.41E-9	17.1	2.49E-9	4.24E-12	485
0.4	5.4E-5	16	2.56E-9	19.8	5.91E-9	7.75E-12	364
0.5	1.3E-4	8.3	2.04E-9	22.1	1.15E-8	1.18E-11	291
0.7	5.1E-4	3.0	1.46E-9	26.2	3.17E-8	2.31E-11	208
1.0	2.1E-3	1.04	1.02E-9	31.3	9.23E-8	4.72E-11	146
1.5	1.1E-2	0.31	6.81E-10	38.3	3.12E-7	1.06E-10	97
2.0	3.4E-2	0.13	5.11E-10	44.2	7.38E-7	1.89E-10	73
3.0	0.171	0.039	3.41E-10	54.2	2.49E-6	4.24E-10	49
4.0	0.541	0.0163	2.56E-10	62.6	5.91E-6	7.55E-10	36
5.0	1.32	0.0083	2.04E-10	69.9	1.15E-5	1.18E-9	29.1
6.0	2.74	0.0048	1.70E-10	76.6	1.99E-5	1.70E-9	24.3
7.0	5.07	3.0E-3	1.46E-10	63	3.17E-5	2.31E-9	20.8
8.0	8.65	2.0E-3	1.28E-10	89	4.73E-5	3.02E-9	18.2

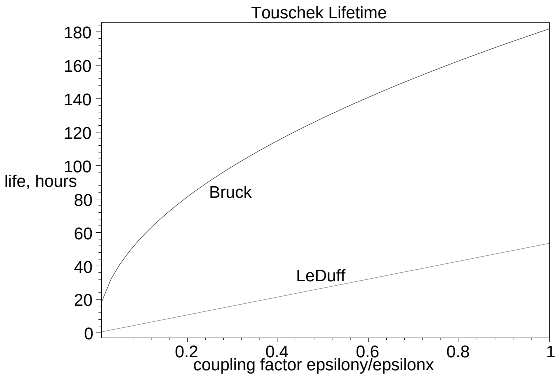

FIGURE 10. Beam lifetime caused by the Touschek effect. $L_C = 6\,\mathrm{m}$, $\epsilon_x = 4.0 \times 10^{-10}\,\mathrm{m}$, $E_0 = 5.0\,\mathrm{GeV}$, $\sigma_z = 0.1\,\mathrm{m}$, $N_B = 1280$.

For the ERL this has assumed a round $2\,\mu$m-emittance beam from the gun, with no further emittance growth throughout the ERL. For RC the same beam from the gun has been assumed, as well as a (more or less arbitrary, but *in principle* achievable) emittance ratio $\epsilon_x/\epsilon_y \approx 100$. For the 8 GeV RC entries the same lattice as for 5 GeV is used. This is probably too optimistic as weaker focusing will probably be required for 8 GeV operation.

If the gun emittance exceeds its specification by, say, a factor of two, $\mathcal{B}_{\mathrm{ERL}}$ falls by a factor of 4. But $\mathcal{B}_{\mathrm{RC}}$ need not fall by the same factor. In fact, if the injection energy has been designed high enough to accept the increased gun emittance, and the charge per bunch specification is met, the RC spectral brightness would be unchanged.

TABLE 4. Comparison of spectral brightnesses $\mathcal{B}$ for various storage-ring-plus-undulator x-ray sources. "RC" stands the present rapid cycling proposal. For this and for the Cornell-ERL case, a 4 meter long, 117 pole, $K = 1$, undulator, with $\lambda_w = 3.4\,$cm, is assumed, and Eq. (1) is used to calculate $\mathcal{B}$. All entries are in the same (standard) units for spectral brightness, given in that equation. For the ESRF and SPRING-8 undulators are similar, but different, and the entries are published values for $\mathcal{B}$. Cases with $\sim$ symbols are obtained by crude scaling. Some possible sources of overestimate in the RC 5 GeV column are discussed in the next section.

E_γ keV	n	RC 5 GeV 4 m	RC 8.1 GeV 4 m	Cornell-ERL 5 GeV 4 m	ESRF, U35 6 GeV	SPRING-8 8 GeV 5 m
4.7	1	7.2E22		∼4E20	6E20	
14	3	∼7E22		∼4E20	5E20	
23	5	∼5E22				
12.4	1		1.1E22			6E20
37.2	3		∼1E22			5E20

Some other spectral brightness comparisons are shown in Table 4. For typical undulators and typical x-ray energies, the spectral brilliance achievable with the proposed rapid cycling scheme is as much as two orders of magnitude greater than the so-called "third generation" light sources, ESRF and SPRING-8. (Different assumptions have undoubtedly gone into the calculations/measurements for these latter data.)

10.2. Refinement of Spectral Brightness Calculation. *This section includes qualifications suggested by (but not necessarily endorsed by) Ivan Bazarov. The central question is whether or not ϵ_y is unnecessarily small in the proposed RC design.*

The entries in Table 4 for potential Cornell x-ray sources are based on Eq. (1). This formula has the benefit of simplicity and definiteness, but it also hides certain physical properties of undulator radiation that enter into assessing the relative effectiveness of different configurations. Some physical considerations not incorporated in Eq. (1) are:

- As was explained in the first section, the main way a storage ring maximizes spectral brightness $\mathcal{B}$ is by minimizing a six-dimensional phase space volume $\mathcal{V}_3\mathcal{P}_3$ which contains most of the produced photons. As $\mathcal{V}_3\mathcal{P}_3$ gets smaller and smaller, the fraction of experiments that can take full advantage of such a small value of $\mathcal{V}_6$ decreases. This means, for example, that many experiments cannnot really exploit some part of the two orders of magnitude decrease in ϵ_y that gives the RC is brightness advantage over the ERL.
- For ultralow emittance beams the radiation may be "diffraction limited". Many of the hypermodern applications of x-rays rely on the coherence properties of beams in this limit. Near a beam waist, either transverse

dimension of the electron beam envelope evolves as

$$y(s) = \sqrt{\epsilon_y \beta_0}\sqrt{1 + \left(\frac{s}{\beta_0}\right)^2}. \tag{30}$$

As such, the parameter β_0 can be referred to as "waist length" or "doubling length". This variation resembles the s-variation of the envelope function w of an electromagnetic wave having wave number $k = 2\pi/\lambda$, in its lowest round, open cavity mode, near a point focus;[**10**]

$$w(s) = w_0\sqrt{1 + \left(\frac{s}{w_0^2 k/2}\right)^2}. \tag{31}$$

For electron and photon beams having the same (round) aspect ratio there is a wave number $k_{\rm dl}$ for which these shapes superimpose. Its corresponding wavelength $\lambda_{\rm dl}$ is given by

$$\lambda_{\rm dl} = \pi\epsilon_0. \tag{32}$$

Another way of obtaining this result is to express the transverse phase space volume of the photon beam (matched to the electron beam) as

$$\mathcal{V}_2^T \mathcal{P}_2^T = \left(\pi\epsilon_0 \frac{h}{\lambda}\right)^2. \tag{33}$$

Condition (32) makes this equal to h^2 which is the phase space volume of one state. This gives, for example for $\lambda_{\rm dl} = 1.0 \times 10^{-10}\,$m, a diffraction limited emittance $\epsilon_0 = 0.3 \times 10^{-10}\,$m. This means that, for a typical x-ray energy of 12 keV, the vertical emittance yielding the RC brightness in Table 4 is unnecessarily small by a factor of 20; the RC brightness value is too high by this factor. For operation above $E_e = 5\,$GeV the estimated brightness becomes more nearly valid.

The degree of transverse coherence is related to $\lambda_{\rm dl}$. For wavelengths much longer than $\lambda_{\rm dl}$ all electrons radiate with transverse coherence. For wavelengths much shorter than $\lambda_{\rm dl}$ the electrons radiate with negligible transverse coherence. For the RC vertical emittance the vertical coherence remains excellent for all x-ray energies and the horizontal coherence is good up to a few keV.

- Spectral brightness $\mathcal{B}$ has been taken to be proportional to the number of undulator periods N_w. This may be surprising when the electric field amplitude radiated at a fixed angle is proportional to N_w, making the intensity (to which the photon flux is proportional) proportional to N_w^2 at the center of an undulator resonance line. It is therefore possible to design a beamline giving flux proportional to N_w^2, though this is not typical. For apparatus with energy acceptance broader than the undulator line, the N_w^2 peak intensity and the $1/N_w$ line width produce flux proportional to N_w, as given by Eq. (1).
- Most x-ray experiments require x-rays as nearly monochromatic as possible, and the feature of undulator radiation to be exploited is that the line width (in energy) is proportional to $1/N_w$. Commonly there is a monochromator near the front of an x-ray beamline. Even for very large,

but realistic, values of N_w, the monochromator fractional energy acceptance is typically far less than $1/N_w$. Even in this case the x-ray flux down the beam line is usually proportional to N_w. This will be true when the angular spread of the electron beam is larger than the x-ray beam collimation is matched to the (post-monochromator) radiation cone of the undulator radiation;

$$\sqrt{\frac{\epsilon}{\beta}} > \frac{1}{\gamma}\sqrt{\frac{1}{nN_w}}, \tag{34}$$

where n is the undulator resonance order. Consider a collimation system centered on the undulator axis and narrowly matched to the central undulator resonance "spike". The probability that a particular radiating electron lines up with this collimation is proportional to $1/N_w$. In this case Eq. (1) continues to be approximately valid. For $\epsilon_x \approx 10^{-10}$ and $\beta_x = 1\,\mathrm{m}$ at the undulator described by Table 4, this inequality is typically satisfied. But for $\epsilon_y \approx 10^{-12}$ the electron vertical angular divergence is smaller than the undulator collimation, again possibly making the spread of vertical electron angles unnecessarily small and making the spectral brightness estimate in Table 4 unduly optimistic. But, in this region the undulator radiation flux is more complicated, for example giving undulator flux density proportional to N_w^2. In short, the performance of any particular physical setup depends on details far too complicated to be accurately described by a simple formula like Eq. (1); this formula may give either an underestimate or overestimate, depending on conditions.

- The fractional energy width of the RC electron beam at 5 GeV is $\sigma_\delta = 0.00066$. The energy spread of the ERL is expected to be 0.0002. Formula (1) does not take into account the improvement in spectral brightness that could result in the ERL by exploiting this advantage by allowing longer undulators. Ivan points out that, as an example, this could permit full brightness for $N_w = 1000$ in the ERL, but only $N_w = 200$ in RC. In any case, at most two such undulators could be incorporated in RC, while more than two could be incorporated in ERL.
- Practical accelerator considerations make it difficult to use very long undulators. In particular both β-functions have to be comparable with or larger than the undulator length. The excellent match of electron beam to photon cone (see Eqs. (30) and (31)) is applicable at the beam waist, but "detunes" elsewhere. The angular spread of electron beam angles is constant through a drift section, but the effective spot size increases away from the waist, and with it the effective emittance. In the RC design, the extremely small value of ϵ_y makes it possible to preserve the diffraction limited condition even for undulator length appreciably longer than β. The ERL will not have this advantage but, because of its less-constrained geometry, it may not need it.
- When the proposed setup is regarded as R&D for the ILC, the extremely small ϵ_y performance is very appropriate.

Bibliography

[1] S. Krinsky, article *Fundamentals of Hard X-Ray Synchrotron Radiation Sources*, in *T*hird Generation Hard X-Ray Synchrotron Radiation Sources, D. Mills editor, John Wiley, New York, 2002

[2] I. Bazarov and C. Sinclair, PRST-AB, **8**, 034202 (2005)

[3]

[4] M. Borland et al., SLAC Report-402 (1991)

[5] R. Sheffield et al., PAC 95, p. 882

[6] D. Trbojevic and E. Courant, *Low emittance lattices for electron storage rings, revisited,* in Proc. EPAC94, p. 1000

[7] H. Bruck, *A*ccélérateurs Circulaires de Particules

[8] C. Bocchetta, *L*ifetime and Beam Quality in CERN 98-04

[9] Y. Miyahara, IEEE Trans. Nucl. Sc., **32**, 3821 (1985)

[10] L.Mandel and E. Wolf, *Optical Coherence and Quantum Optics*, Cambridge University Press, p.269, 1995